Article ID:0253-2778(2014)08-0623-14

Rhodanine-containing fullerene derivative as a new acceptor in polymer solar cells with enhanced light absorption

XIE Lixin[1], ZHAO Xuemei[1], ZHAO Zhiqiang[1], ZHEN Jieming[1], CHEN Muqing[1], ZHU Jun[2], DAI Songyuan[2], YANG Shangfeng[1]

(1. *Hefei National Laboratory for Physical Sciences at Microscale, CAS Key Laboratory of Materials for Energy Conversion, Department of Materials Science and Engineering, University of Science and Technology of China, Hefei* 230026, *China*;
2. *Key Laboratory of Novel Thin Film Solar Cells, Institute of Plasma Physics, Chinese Academy of Sciences, Hefei* 230031, *China*)

Abstract: A dye unit, 3-ethyl rhodanine, was attached onto (6,6)-phenyl-C61 butyric acid methyl ester (PCBM) for the first time, affording a new fullerene acceptor PCBM-rhodanine (PCBRh) for polymer solar cells (PSCs) with enhanced light absorption. The successful attachment of the rhodanine moiety was confirmed by ^{1}H NMR, ^{13}C NMR and matrix-assisted laser desorption/ionization time-of-flight (MALDI-TOF) mass spectroscopies. UV-vis spectroscopic study indicated that PCBRh had stronger absorptions in the region of 300～600 nm than PCBM, and this was due to the high absorption coefficient of the dye unit of 3-ethyl rhodanine. Cyclic voltammetric measurement revealed that the lowest unoccupied molecular orbital (LUMO) level of PCBRh was 0.1 eV higher than that of PCBM, which can be understood by considering the electron donating property of the rhodanine moiety. Using PCBRh as an acceptor blending with poly(3-hexylthiophene-2,5-diyl) (P3HT), the bulk heterojunction (BHJ) PSC device exhibited a power conversion efficiency (PCE) of 1.46% under the optimized condition (blending ratio of P3HT:PCBM=1:1 (mass ratio), annealing treatment at 135 ℃ for 10 min). The effect of annealing on the morphology of P3HT:PCBRh active layer and its correlation with the device performance were studied by atomic force microscopy (AFM), revealing that in the annealed P3HT:PCBRh blend film P3HT aggregated to long stripes with an average length of ca. 20 nm and the RMS roughness increased compared to that for the reference P3HT:PCBM blend film, thus leading to unfavorable exciton diffusion and dissociation.

Key words: polymer solar cell; fullerene; functionalization; 3-ethyl rhodanine; (6,6)-phenyl-C61 butyric acid methyl ester (PCBM)

CLC number: TQ050.4+22 **Document code**: A doi:10.3969/j.issn.0253-2778.2014.08.001

Citation: Xie Lixin, Zhao Xuemei, Zhao Zhiqiang, et al. Rhodanine-containing fullerene derivative as a new acceptor in polymer solar cells with enhanced light absorption[J]. Journal of University of Science and Technology of China, 2014,44(8):623-636.

Received: 2014-05-09; **Revised**: 2014-05-20

Foundation item: Supported by National Natural Science Foundation of China (21132007, 21371164), Key Project of Hefei Center for Physical Science and Technology (2012FXZY006).

Biography: XIE Lixin, female, born in 1989, master. Research field: polymer solar cells, carbon nanomaterials. E-mail: xielixin@mail.ustc.edu.cn

Corresponding author: YANG Shangfeng, PhD/Prof. E-mail: sfyang@ustc.edu.cn

绕丹宁修饰富勒烯作为新型聚合物太阳能电池受体光伏材料增强光吸收

谢丽欣[1],赵雪梅[1],赵志强[1],甄杰明[1],陈木青[1],朱 俊[2],戴松元[2],杨上峰[1]

(1.中国科学技术大学材料科学与工程系,合肥微尺度物质科学国家实验室,中国科学院能量转换材料重点实验室,安徽合肥 230026;
2.中国科学院新型薄膜太阳能电池重点实验室,中国科学院等离子体物理研究所,安徽合肥 230031)

摘要:首次将染料分子 3-乙基绕丹宁连接到[6,6]-苯基-C_{61}-丁酸甲酯(PCBM)上,合成了具有增强光吸收性能的新型富勒烯受体光伏材料 PCBRh.通过^{1}H NMR,^{13}C NMR 和质谱分析确定了 PCBRh 的结构,紫外-可见吸收光谱测试表明所合成的 PCBRh 在 300～600 nm 比起 PCBM 具有更强的光吸收,这归因于 3-乙基绕丹宁高的吸光系数.电化学测试表明 PCBRh 的最低未占轨道(LUMO)能级比 PCBM 高 0.1 eV,这是由绕丹宁基团的给电子作用引起的.将 PCBRh 作为受体光伏材料与聚己基噻吩(P3HT)共混构建出体相异质结太阳能电池,在优化的制备工艺(P3HT/PCBRh=1:1(质量比),135 ℃热处理 10 min)下,电池器件的能量转换效率为 1.46%.通过 AFM 表征研究退火处理对光活性层的形貌的影响及其与电池器件效率的联系:与参比 P3HT:PCBM 共混薄膜相比,退火处理使 P3HT:PCBRh 薄膜中的 P3HT 聚集成长度约为 20 nm 的长条,并且粗糙度较大,因此不利于激子的扩散与分离.

关键词:聚合物太阳能电池;富勒烯;功能化;3-乙基绕丹宁;[6,6]-苯基-C_{61}-丁酸甲酯(PCBM)

0 Introduction

Polymer solar cells (PSCs) have been regarded as a clean and renewable energy source with the advantage of easy fabrication, low cost, light weight, synthetic variety and mechanical flexibility[1-5]. The bulk heterojunction (BHJ) PSC devices are composed of an active layer of a conjugated polymer donor such as poly (3-hexylthiophene-2,5-diyl) (P3HT) and a soluble acceptor typically [6,6]-phenyl-C61-butyric acid methyl ester ($PC_{61}BM$) sandwiched between an anode and a cathode[6-8]. The photovoltaic materials of both conjugated polymer donor and fullerene acceptor with broad visible to NIR absorption, high charge carrier mobility, and matching of energy levels are crucial for high performance of PSCs[9-12]. During the past decade, a number of novel low band-gap polymers were synthesized by employing the donor-acceptor (D-A) approach and power conversion efficiency (PCE) of the corresponding BHJ-PSC devices have surpassed 9% based on such donor polymer as thieno [3,4-b]-thiophene/benzodithiophene (PTB7) and [6,6]-phenyl-C71-butyric acid methyl ester ($PC_{71}BM$)[13-14]. However, acceptor materials for PSCs have been less studied[5,11]. Since the first report by Hummelen et al.[15], $PC_{61}BM$ (hereafter abbreviated as PCBM) has remained the most commonly used acceptor material for good solubility in common organic solvents, high electron mobility and high electron affinity[5,11-12]. However, PCEs of the reported PCBM-based PSC devices have so far still been limited due to its low-lying energy level with poor matching with that of the typical donor and weak absorption in the visible region[5,11-12]. Thus, it is desirable to develop new acceptors with improved energy level matching and/or light absorption.

Up to now, two general approaches have been developed to functionalize fullerenes as better acceptors for PSCs. One is to raise its lowest unoccupied molecular orbital (LUMO) energy level by attaching electron-donating groups onto fullerenes[5,11], synthesizing fullerene bisadducts[16-21] or substituting empty fullerenes with endohedral fullerenes[22]. For instance, indene-C_{60} bisadduct (ICBA) exhibited a LUMO level 0.17 eV higher than that of PCBM and a stronger absorption in the visible region, and the

BHJ-PSC device based on ICBA acceptor blended with P3HT showed dramatically improved open circuit voltage (V_{oc}) (0.84 V) and PCE (5.44%) compared to those of the P3HT:PCBM device[18]. Similarly, LUMO of dihydronaphthyl-based C_{60} bisadduct ($NC_{60}BA$) was 0.16 eV higher than that of PCBM, and the BHJ-PSC device based on P3HT:$NC_{60}BA$ exhibited better performance with higher V_{oc} of 0.82 eV and PCE of 5.37%[17]. However, these fullerene bisadducts are the mixture of multiple isomers, hindering the effective packing of molecules required for efficient electrons transport, and the separation of individual isomers is quite tedious[23-24]. Another remarkable example to raise the LUMO level of fullerene acceptors was to use endohedral fullerenes such as $Lu_3N@C_{80}$ to replace empty fullerene C_{60}, and LUMO of $Lu_3N@C_{80}$-PCBH (H=hexyl) was 0.28 eV higher than that of PCBM. As a result, V_{oc} of the corresponding P3HT:$Lu_3N@C_{80}$-PCBH devices was increased by 0.26 eV compared to that of the P3HT:PCBM devices and the optimized PCE reached 4.2%[22]. In this case, nevertheless, the rarity and high cost of endohedral fullerenes would inevitably limit the common use.

Another approach toward novel fullerene acceptors for PSCs is to enhance its light absorption. For instance, $PC_{71}BM$ shows a significantly higher absorption coefficient in the visible region and thus results in better performance in PSCs compared to $PC_{61}BM$[25]. Recently, a new method has been developed to enhance light absorption of fullerene acceptors by attaching dyes as the end unit via esterification reaction[26-27]. A novel fullerene acceptor F based on modification of PCBM with 4-nitro-4′-hydroxy-α-cyanostilbene (NHCS) was reported[27]. With enhanced light absorption and a higher LUMO level compared to that of PCBM, P3HT:F BHJ-PSC devices exhibited a PCE of 4.23%, much higher than that based on P3HT:PCBM (2.93%), while PCE of P3HT:F device was further improved to 5.25% upon treatment with acetone additive and thermal annealing[27].

In this paper, 3-ethyl rhodanine, recently demonstrated by Li et al.[28-30] as an effective dye to enhance light absorption of small-molecule donors for BHJ-PSCs, was successfully attached onto PCBM for the first time, affording a new acceptor (PCBRh) for PSCs with enhanced light absorptions in the region of 300～600 nm. Cyclic voltammetric measurement was carried out to investigate the influence of the rhodanine moiety on the molecular orbitals of PCBRh. The photovoltaic property of PCBRh was studied by fabricating BHJ-PSC devices based on PCBRh blending with P3HT, and the correlation between the morphology of the active layer and performance was unveiled.

1 Experimental

1.1 Materials

All solvents and reagents were commercially available and used as received without further purification. P3HT and PCBM were bought from Luminescence Techology Corp. and Nichem Fine Technology Co., Ltd., respectively. 1-(3-Carboxypropyl)-1-phenyl[6,6]C61-butyric acid (PCBA) was synthesized by treating PCBM with HCl and acetic acid following the literature method[15].

1.2 Measurements

Column chromatography (CC): SiO_2 (300～400 mesh). UV-Vis spectra were measured on a UV-3600 spectrometer (Shimadzu, Japan) using a quartz cell of 10 mm layer thickness and 1 nm resolution. ^1H NMR spectra and ^{13}C NMR spectra were recorded on a Bruker AV400 or AV300 NMR instrument using tetramethylsilane as an internal reference. The mass spectra were recorded by matrix-assisted laser desorption/ionization time-of-flight (MALDI-TOF) mass spectroscopy (Biflex Ⅲ, Bruker Daltonics Inc., Germany). Thermogravimetric analysis (TGA) was recorded on a TGA Q5000 Instrument under nitrogen

atmosphere at a heating rate of 10 ℃/min. Photoluminescence (PL) spectra were measured using an F-4600 FL Spectrophotometer. Atomic force microscopy (AFM) images were taken using a Nanoscope Ⅲ (Digital Instruments, USA) operating in both height and phase modes. Cyclic voltammetry was conducted on a CHI 660D Electrochemical Workstation (CHI Instrument, USA) with Pt disk, Pt wire, and Ag electrode used as working electrode, counter electrode, and reference electrode, respectively, in a 0.1 mol/L tetrabutylammonium hexafluorophosphate ($[^nBu_4N]^+[PF_6]^-$, $TBAPF_6$) in o-dichlorobenzene solution, scan rate: 100 mV/s.

1.3 Synthesis

The synthetic route of PCBRh is shown in Scheme 1. The detailed synthetic procedures are as follows:

(Ⅰ) 5-(4-hydroxybenzylidene)-3-ethyl-rhodanine (Rh-OH)

This compound was synthesized by Knoevenagel condensation[28,31]. 3-ethyl rhodanine (10.0 mmol, 1.61 g) and sodium acetate (10 mmol, 0.77 g) were added to 50 mL acetic acid and heated to 80 ℃ in an oil-bath for 5 min. Then 4-hydroxybenzaldehyde (10.0 mmol, 1.22 g) was added to the hot acid. After a period of 12 h reflux, the reaction was stopped, and a crystalline product was achieved after cooling to room temperature. The mixture was poured into water (30 mL) for precipitation and the solid was filtered. Then the crude compound was purified by recrystallization in ethanol, affording a yellow solid (45% yield). ^{1}H NMR (300 MHz, $CDCl_3$) δ 7.70 (s, 1H), 7.45 (d, J=8.7 Hz, 2H), 7.01～6.85 (m, 2H), 5.28 (s,1H), 4.22 (q, J=7.1 Hz, 2H), 1.31 (t, J=7.1 Hz, 3H). ^{13}C NMR (75 MHz, $CDCl_3$) δ 193.16, 167.79, 158.16, 132.70, 126.19, 120.45, 116.72, 39.79, 12.39. MALDI-TOF MS m/z calculated for $C_{12}H_{11}NO_2S_2$: 265.02, found: 265.02.

(Ⅱ) PCBRh

N,N′-dicyclohexylcarbodiimide (DCC) (0.18 mmol, 37 mg) was added to a pre-cooled 20 mL CS_2 solution of PCBA (0.09 mmol, 82 mg), Rh-OH (0.27 mmol, 71 mg) and a catalytic amount of 4-dimethylaminopyridine (DMAP) (0.07 mmol, 8 mg). The mixture was stirred overnight at room temperature. After evaporation under reduced pressure, the residue was purified by column chromatography (silica gel, toluene: CS_2 = 1:4). The obtained product was further precipitated in methanol affording pure product as a dark-brown solid (66% yield). ^{1}H NMR (400 MHz, $CDCl_3$) δ 8.01～7.85 (m, 2H), 7.68 (s, 1H), 7.61～7.43 (m, 5H), 7.21 (d, J=1.9 Hz, 1H), 7.20 (d, J=1.8 Hz, 1H), 4.19 (q, J=7.1 Hz, 2H), 3.10～2.90 (m, 2H), 2.80 (t, J=7.4 Hz, 2H), 2.44～2.22 (m, 2H), 1.31 (t, J=7.1 Hz, 3H). ^{13}C NMR (75 MHz, $CDCl_3$) δ 192.96 (C=S),

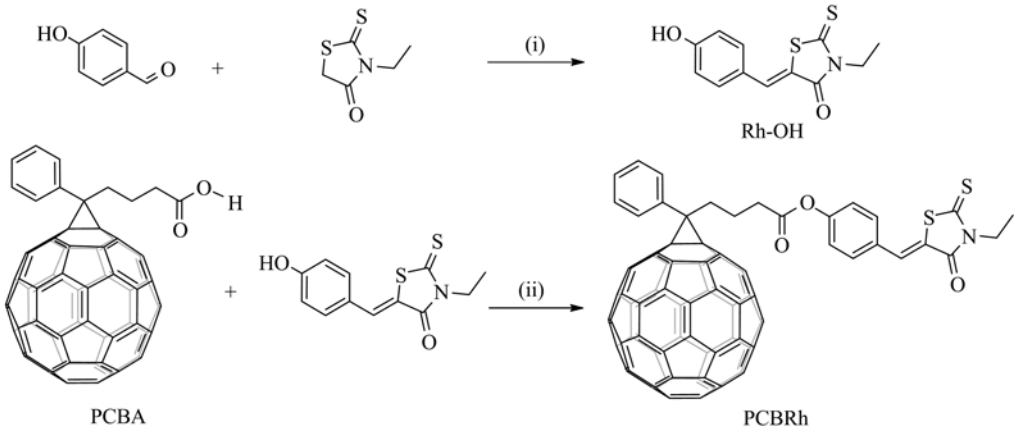

(ⅰ) CH_3COONa, CH_3COOH, 80 ℃; (ⅱ) DMAP, DCC, CS_2, room temperature

Scheme 1 Synthetic route of PCBRh

171.17 (C = O), 167.67 (C = O), 152.26, 148.82, 147.79, 145.95, 145.36, 145.33, 145.21, 145.18, 144.96, 144.83, 144.68, 144.59, 144.18, 143.90, 143.32, 143.21, 143.17, 143.10, 143.07, 142.35, 142.32, 142.28, 142.25, 141.19, 140.93, 138.18, 137.75, 136.80, 133.16, 132.26, 131.98, 131.83, 131.21, 129.18, 128.68, 128.51, 128.37, 123.53, 122.75, 121.70, 79.87 (sp^3-C of C_{60}), 51.75 (PhC), 40.00 (N-C), 34.31 ($PhCCH_2$), 33.73 (CH_2CO_2), 22.42 (CH_2CCO_2), 12.41 (CH_3). MALDI-TOF m/z calculated for $C_{23}H_{23}NO_3S_2$: 1 143.10, found: 1 143.78.

1.4 Device fabrication and measurements

The fabrication procedure of P3HT:PCBRh BHJ-PSC devices is similar to that used for the reference P3HT:PCBM devices reported previously[32-38]. Briefly, the ITO-coated glass substrate (8 Ω per square, purchased from Shenzhen Nan Bo Group, China) was first cleaned with detergent, then ultrasonicated in acetone and 2-propanol, and subsequently dried in vacuum at 60 ℃ overnight. PEDOT:PSS (Baytron P) layer (~ 35 nm thick) was spin-coated onto the ITO substrate and then annealed at 120 ℃ for 30 min. The P3HT:PCBRh blend with variable mass ratio (1:0.6 to 1:2) was dissolved in o-dichlorobenzene by stirring at 40 ℃ overnight, which was spin-coated onto the PEDOT:PSS layer affording the P3HT:PCBRh active layer (~100 nm thick). All of the solution processing and film preparation were carried out in air atmosphere. Then the wet P3HT:PCBRh films were covered by a glass petri dish under nitrogen atmosphere for 2 h to undergo solvent annealing process. The device was next transferred into a vacuum chamber (~1.33×10^{-3} Pa), and an Al electrode (~ 100 nm thick) was deposited on the top of the active layer through a shadow mask to the active area of the devices (2×5 mm^2). Finally, thermal annealing was carried out at 135 ℃ for 10 min on a digital hot plate in a nitrogen atmosphere inside a glove box. PCE was measured under simulated AM 1.5G irradiation (100 $mW\cdot cm^{-2}$) using a standard xenon-lamp-based solar simulator (Oriel Sol 3A, USA), for which the illumination intensity was calibrated by a monocrystalline silicon reference cell (Oriel P/N 91150V, with KG-5 visible color filter) calibrated by the National Renewable Energy Laboratory (NREL). The current-voltage (*J-V*) characteristics were measured with a Keithley 2 400 source meter. All the measurements were carried out in air atmosphere and a mask with well-defined area of 10.0 mm^2 was attached onto the cell to define the effective area to ensure measurement accuracy. More than ten devices were fabricated independently under each experimental condition and measured to ensure data consistency, and the average results were used in the following discussions. The External quantum efficiency (EQE) curves were measured by using an IQE measurement system (ORIEL 200™).

2 Results and discussion

2.1 Synthesis and characterization of PCBRh

Recently, Li et al.[28] developed a new small-molecule donor in BHJ-PSCs by introducing 3-ethyl rhodanine as the end unit and achieved a high PCE of 6.1%, which was even higher than that of the landmark PCE at that time due to the high absorption coefficient of the dye unit of 3-ethyl rhodanine. To our knowledge, so far the rhodanine unit has not been integrated in the acceptor in BHJ-PSCs despite its excellent light absorption property. Thus, in the present work we managed to incorporate 3-ethyl rhodanine into PCBM as the end group for the first time, and the synthetic route of PCBRh is shown in Scheme 1. PCBRh was synthesized facilely by two-step reactions: in the first step, 3-ethyl rhodanine reacted with 4-hydroxybenzaldehyde via Knoevenagel condensation affording Rh-OH[28,31], which was then covalently attached onto PCBA via an esterification reaction in the second step[34-35].

The molecular structure of PCBRh was characterized by ^1H NMR, ^{13}C NMR and MALDI-

TOF mass spectroscopies. Fig. 1 shows the ^{1}H NMR spectrum of PCBRh (curve a) in comparison with those of PCBM (curve b) and Rh-OH (curve c). As clearly seen in Fig. 1, the characteristic proton signal of the hydroxyl group ($\delta = 5.28$ ppm) of Rh-OH disappears in PCBRh and the proton signal of H (g) is down-field shifted as a result of the electron withdrawing resonance from ester group, indicating the successful esterification between Rh-OH and PCBM.

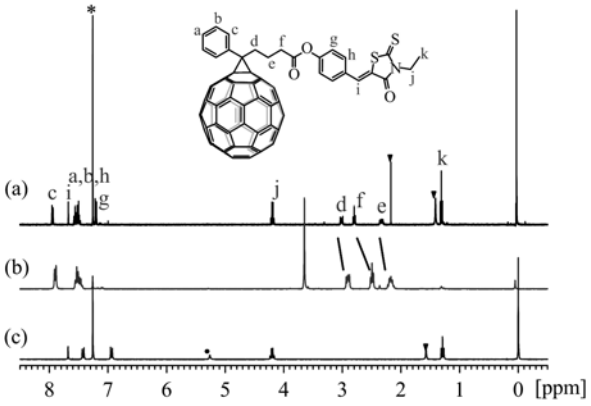

All compounds were dissolved in deuterated chloroform and the spectra were recorded at room temperature. The solvent line of $CHCl_3$ is marked with an asterisk. The filled inverted triangles label the signal lines from the residual CH_3OH and H_2O solvents. The filled circle in curve (c) labels the proton signal of the hydroxyl group of Rh-OH.

Fig. 1 ^{1}H NMR spectra of PCBRh (a), PCBM (b) and Rh-OH (c)

Substitution of the end group of PCBM avoids dramatic perturbation of its electronic structure as reported in literatures[39-40]. The ^{1}H NMR spectrum of PCBRh is further compared to that of PCBM specifically the proton signals of the three methylene (-CH_2-, H(d)-H(f)) groups between the carbonyl group and cyclopropane ring. Noteworthily, the proton signal of H(f), which is closest to the rhodanine moiety, is evidently down-field shifted relative to that of PCBM, and this is due to the deshielding effect caused by the ring current effect of the anisotropic phenyl group of Rh-OH[41]. Contrarily, the proton signals of H(e) and H(d) are only slightly shifted due to their longer distance to the Rh-OH moiety.

In the ^{13}C NMR spectrum of PCBRh (Fig. 2), $\delta = 120 \sim 160$ ppm can be assigned to the sp^2 carbon atoms of C_{60} in combination with those of the phenyl and ethenyl groups. On the other hand, among the seven sp^3 carbon lines found in the 10～90 ppm regions, the signals at $\delta = 51.75$ and 79.87 ppm could be assigned to the bridged carbon of the cyclopropane ring formed via [6,6]-addition of C_{60} and the fullerenyl sp^3 carbon, respectively[15].

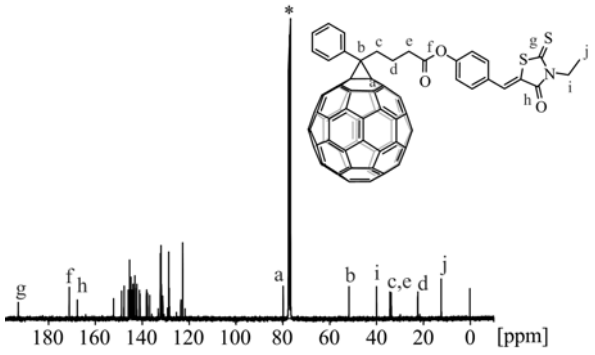

The sample was dissolved in deuterated chloroform and the spectrum was recorded at room temperature. The solvent line of $CHCl_3$ is marked with an asterisk. The signals in the region of 120～160 ppm are assigned to the sp^2 carbon lines of C_{60} combined with those of two phenyl groups.

Fig. 2 ^{13}C NMR spectrum of PCBRh

TGA analysis shows that PCBRh possesses a high thermal stability with a decomposition temperature of up to 341 ℃. At the decomposition temperature, PCBRh losses weight of around 20% suddenly (Fig. 3). This weight loss is consistent well with the mass ratio of Rh-OH moiety in PCBRh molecule.

2.2 Electronic absorption and photoluminescence properties of PCBRh

Fig. 4(a) compares the UV-vis absorption spectra of PCBRh, PCBM and Rh-OH in toluene with a concentration of 1.0×10^{-5} mol/L. Clearly, the absorption spectrum of PCBRh shows a superposition of those of PCBM and Rh-OH. Compared to PCBM, PCBRh shows significantly stronger absorption in the region of 300～600 nm (see inset of Fig. 4 (a)), and this is due to the

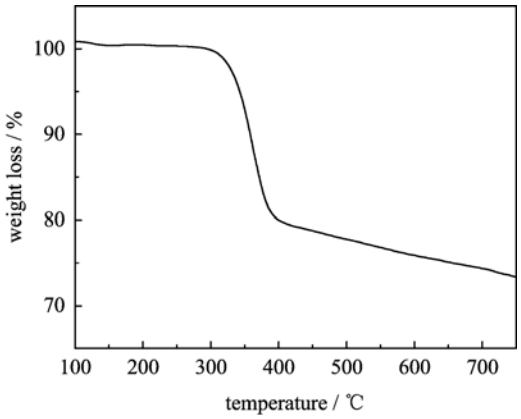

Fig. 3　Thermogravimetric analysis (TGA) curve of PCBR with a heating rate of 10 ℃/min under N_2

high absorption coefficient of the dye unit of 3-ethyl rhodanine[28]. The four absorption maxima (λ_{max}) of PCBRh are observed at 330, 371, 386 and 433 nm (Tab. 1). Among them, the latter absorption peak at 433 nm is clearly observed in the spectrum of PCBM as well, which is characteristic of [6, 6]-addition of C_{60}[40,42]. Besides, the optical band-gap ($E_{g,opt}$) of PCBRh estimated from the absorption spectral onset of ca. 704 nm is 1.76 eV, slightly larger than that of PCBM (1.71 eV) (Tab. 1)[43]. On the other hand, λ_{max} of PCBRh at 386 nm is blue-shifted by 13 nm compared to that of Rh-OH (399 nm), suggesting the perturbation of the end unit[44].

Tab. 1　Characteristic electronic absorption and electrochemical data of PCBRh and PCBM

	λ_{max} /nm	λ_{onset} /nm	$E_{g,opt}$[a] /eV	E_{red}^{onset}[b] /V	LUMO[c] /eV	HOMO[d] /eV
PCBRh	330,371, 386,433	704	1.76	−1.18	−3.62	−5.38
PCBM	330,433	725	1.71	−1.08	−3.72	−5.43

【Note】 [a] Based on the UV-vis absorption spectra measured in toluene solution; [b] $E_{g,opt}/eV = 1\,240/\lambda_{onset}$; [c] Potential in volts vs. Fc/Fc^+; [d] LUMO energy levels (E_{LUMO}) were calculated according to the equation: $E_{LUMO} = -e(E_{red}^{onset} + 4.8V)$; [e] $E_{HOMO} = E_{LUMO} - E_{g,opt}$.

The UV-vis absorption spectra of P3HT:PCBRh (1:1, mass ratio) and P3HT:PCBM blend films annealed at 135 ℃ are compared in Fig. 4(b). For all three spectra, the absorption peak at around 550 nm is assigned to π − π *

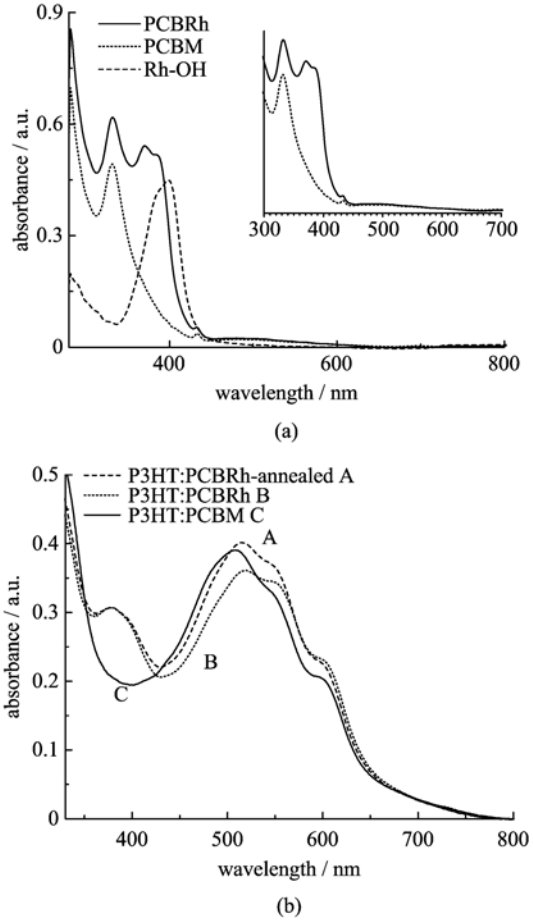

Fig. 4　UV-vis spectra of PCBR, PCBM and Rh-OH in toluene (1.0×10^{-5} mol/L) (a), and UV-vis spectra of P3HT:PCBR and P3HT:PCBM blend films (b)

transition of P3HT, and the absorption shoulder at around 600 nm correlates to the interplay of the interchain of P3HT with the intensity depending on the ordering of the interchain packing[27,45]. Compared to P3HT: PCBM film (curve C), P3HT: PCBRh film (curve B) exhibits higher absorption intensity for the shoulder peak around 600 nm, indicating a better interchain ordering of P3HT within the P3HT: PCBRh blend film[45-46]. Interestingly, after being annealed at 135 ℃, the absorption intensity of P3HT: PCBRh blend film (curve A) in the region of 400～560 nm increases obviously, and this is interpreted by the enhanced degree of crystallinity of P3HT induced by thermal annealing[45]. Besides, in the region of 350～450 nm, P3HT: PCBRh blend film also shows much stronger absorption than that of P3HT: PCBM,

and this, similar to the case of the solution spectrum discussed above, is attributed to the enhanced absorption of PCBRh in this region by the dye unit of 3-ethyl rhodanine[28].

Fig. 5 compares the PL spectra of the unannealed P3HT:PCBRh (1:1) blend film and those of P3HT: PCBM (1: 1) and pure P3HT films excited at 500 nm. Clearly, for PCBM:PCBRh (1: 1) blend film, the blending of PCBRh with P3HT led to a quenching of 91% of the PL emission of P3HT, and this quenching ratio is comparable to that for P3HT: PCBM (1: 1) blend film with a 94% PL quenching. These results indicate that, similar to the case of the well-known P3HT:PCBM system, a strong intermolecular photoinduced electron transfer may occur for the P3HT:PCBRh blend as well, which is crucial for the exciton dissociation in PSCs[1-6].

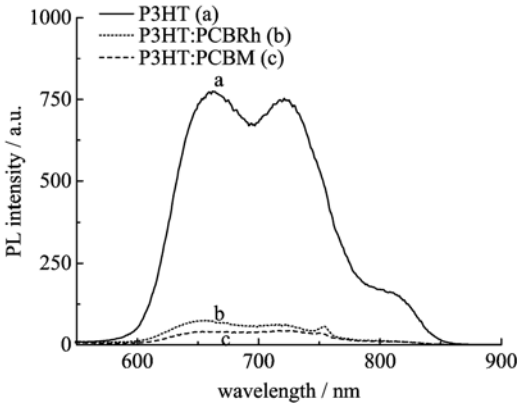

The excitation wavelength was 500 nm.

Fig. 5 Room-temperature PL spectra of P3HT (a), P3HT:PCBRh (1:1) (b) and P3HT:PCBM (1:1) (c) films spin-coated onto ITO

2.3 Electrochemical properties of PCBRh

Electrochemistry is a commonly used technique to probe the energy levels of the molecular orbitals of fullerene derivatives[5,15,47-49]. Fig. 6 illustrates the cyclic voltammogram of PCBRh in comparison with those of Rh-OH and PCBM measured in o-dichlorobenzene. The lowest unoccupied molecular orbital (LUMO) can be calculated according to the equation: $E_{LUMO} = -e(E_{red}^{onset} + 4.8\ V)$, where E_{red}^{onset} is the onset reduction potential in volts versus Fc/Fc^{+}[50]. The E_{red}^{onset} and energy levels of molecular orbitals are summarized in Tab. 1. E_{red}^{onset} of PCBRh and PCBM are −1.18 and −1.08 V versus Fc/Fc^{+}. Accordingly the calculated LUMO of PCBRh and PCBM is −3.62 eV and −3.72 eV, respectively. Interestingly, upon the attachment of the rhodanine moiety, LUMO of PCBRh is raised by 0.1 eV compared to that of PCBM, and this can be understood by considering the electron donating property of the rhodanine moiety[51-52]. Besides, the second reduction peak of PCBRh appears to be the superposition of the corresponding reduction peaks of Rh-OH and PCBM with a negative shift of ca. 0.2 V relative to that of PCBM.

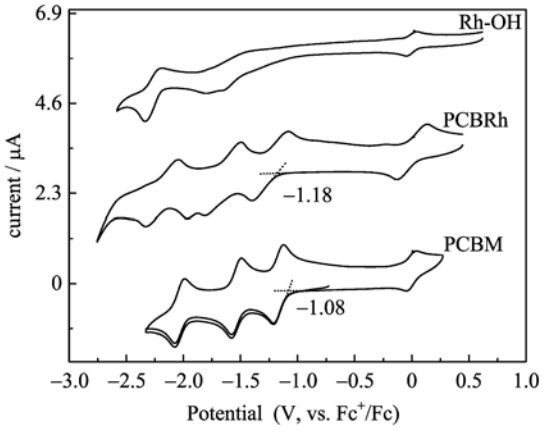

Scan rate: 100 mV/s

Fig. 6 Cyclic voltammograms of PCBRh, PCBM and Rh-OH in o-dichlorobenzene with 0.1 mol/L $TBAPF_6$ as supporting electrolyte

2.4 Photovoltaic properties of PCBRh

To investigate the photovoltaic properties of PCBRh, we fabricated BHJ-PSC devices using PCBRh as an electron acceptor blended with P3HT. The schematic architecture of BHJ-PSC devices (ITO/PEDOT: PSS/P3HT: Acceptor/Al) is shown in Fig. 7 (a). We first optimized the blending ratio of P3HT:PCBRh from 1:0.6 to 1: 2, and found that a blending ratio of P3HT: PCBRh = 1: 1 (mass ratio) afforded the best performance. For comparison, the reference device based on PCBM acceptor was also fabricated under identical conditions (P3HT: PCBM = 1: 1 (mass

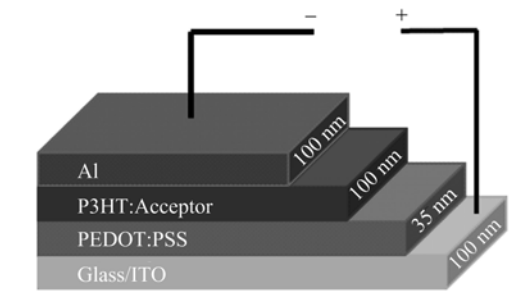

(a) The schematic architecture of ITO/PEDOT:PSS/P3HT:Acceptor/Al BHJ-PSC device

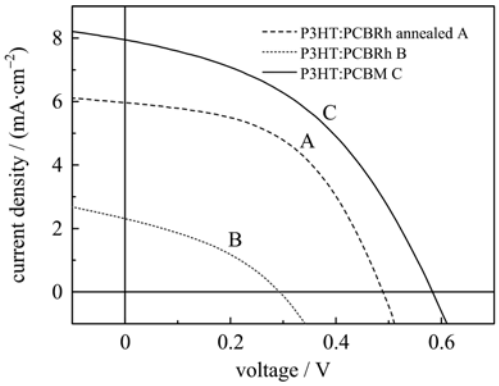

(b) *J-V* curves of the BHJ-PSC devices based on P3HT:PCBR with (A) and without (B) annealing and P3HT:PCBM after annealing (C) as reference

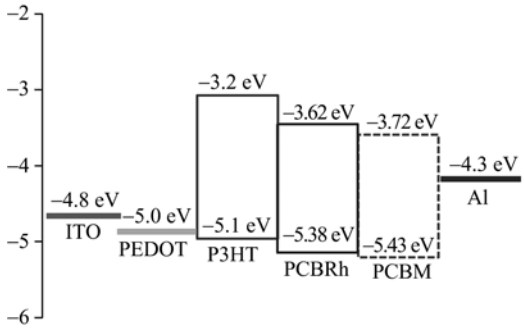

(c) Energy level diagram of ITO/PEDOT:PSS/P3HT:Acceptor/Al BHJ-PSC devices

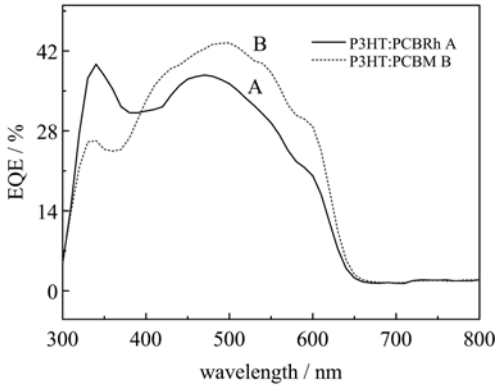

(d) EQE curves of the BHJ-PSC devices based on P3HT:PCBR (A) and P3HT:PCBM (B) after annealing

The measurements were carried out under AM 1.5 G illumination at an irradiation intensity of 100 mW/cm^2

Fig. 7　The structure and characterization of BHJ-PSC devices

ratio))[32-38]. The current density-voltage (*J-V*) curves of the ITO/PEDOT:PSS/P3HT:PCBRh/Al devices (with or without annealing treatment) under the illumination of AM 1.5 G (100 mW/cm^2) is presented in Fig. 7(b), which includes that of the reference ITO/PEDOT:PSS/P3HT:PCBM/Al device as well for comparison, and the measured photovoltaic parameters including V_{oc}, short-circuit current (J_{sc}), fill factor (FF) and PCE are summarized in Tab. 2. Under the optimized blending ratio of P3HT:PCBRh = 1:1 (mass ratio), we found that the device's performance was dramatically enhanced by annealing treatment, and the efficiency enhancement was sensitively dependent on the annealing temperature. As seen in Fig. 7 (b), the pristine ITO/PEDOT:PSS/P3HT:PCBRh/Al device without annealing treatment exhibited a very low PCE of 0.24% (curve B). Upon the optimized annealing treatment at 135 ℃ for 10 min, PCE of the annealed ITO/PEDOT:PSS/P3HT:PCBRh/Al device increases to 1.46% (curve A). Under the identical fabrication and annealing conditions (135 ℃ for 10 min), the reference ITO/PEDOT:PSS/P3HT:PCBM/Al device exhibits a PCE of 2.00% (curve C), much higher than that of the PCBRh-based device.

Tab. 2　Photovoltaic parameters of BHJ-PSCs based on P3HT:PCBM and P3HT:PCBRh

Active layer	V_{oc}/V	J_{sc} /(mA·cm^{-2})	FF	PCE/%
P3HT:PCBM[a]	0.58	7.92	0.43	2.00
P3HT:PCBR	0.29	2.31	0.35	0.24
P3HT:PCBR[a]	0.49	5.96	0.50	1.46

【Note】 [a] annealed at 135 ℃ for 10 min. The measurements were carried out under AM 1.5 G illumination at an irradiation intensity of 100 mW/cm^2.

The External quantum efficiency (EQE) curves of the corresponding devices after annealing are shown in Fig. 7(d). In the UV region from 317 nm to 393 nm, the EQE of PCBRh-based device is significantly higher than that of PCBM-based device due to enhanced light absorption from PCBRh (Fig. 4). However, the case inverses in the visible region, which correlates with the lower J_{sc} in the case of PCBRh-based device.

In order to understand the relatively lower PCE of ITO/PEDOT: PSS/P3HT: PCBRh/Al device compared to that of the reference PCBM-based device, we compared each parameter determining PCE including V_{oc}, J_{sc} and FF in Tab. 2. Clearly, both V_{oc} (0.49 V) and J_{sc} (5.96 mA/cm^2) of the PCBRh-based device (annealed) are lower than those of the PCBM-based one (0.58 V, 7.92 mA/cm^2), leading to the inferior performance of the PCBRh-based device. However, FF of the annealed PCBRh-based device (0.50) shows a considerable increase compared to that of the PCBM-based one (0.43). The trade-off between V_{oc}/J_{sc} and FF suggests a complex mechanism responsible for the inferior performance of the PCBRh-based device, as discussed further below. On the other hand, compared to the un-annealed device, all of the three parameters (V_{oc}, J_{sc}, FF) of the annealed PCBRh-based device increase dramatically, revealing that annealing treatment is crucial for the high performance of the PCBRh-based device.

It is known that V_{oc} is primarily correlated to the difference between the HOMO level of the donor and the LUMO level of the acceptor within the active layer, which may be perturbed by the morphology of the active layer[1-6,53-55]. According to the energy level diagram of ITO/PEDOT:PSS/P3HT:PCBRh (PCBM)/Al device plotted in Fig. 7(c)[5,11,32,34-36,56], the difference between the HOMO level of P3HT (−5.1 eV) and the LUMO level of the PCBRh acceptor (−3.62 eV) is higher by 0.1 eV than that based on PCBM acceptor because of the higher LUMO level of PCBRh as discussed above. In principle, such an increased difference between the HOMO level of P3HT and the LUMO level of the PCBRh acceptor should reduce the energy loss in the exciton dissociation and contribute to the increase of V_{oc}[5,11,51], which however, decreases in our present case. Therefore, the inferior performance of the PCBRh-based device resulting partially from the decrease of V_{oc} should not be attributed to the mismatch of energy level between P3HT donor and PCBRh acceptor.

The surface morphologies of the blend films were studied by AFM in the tapping mode. Fig. 8 compares the AFM images of the P3HT:PCBRh blend films in both height and phase modes before and after annealing treatment, which includes also those of the reference P3HT:PCBM blend film for comparison. As clearly seen in images A and D in Fig. 8, the reference P3HT:PCBM film shows an interpenetrating network of P3HT and PCBM with clear P3HT-rich and PCBM-rich domains due to their microphase separation behavior, and the film surface is quite smooth with a root-mean-square (RMS) roughness of around 0.73 nm. In contrast, for P3HT: PCBRh blend film, a dramatically different surface morphology is observed. In the AFM images of the pristine (un-annealed) P3HT: PCBRh blend film (images B and C in Fig. 8), P3HT molecules appear to aggregate into discrete domains as spots with an average diameter of ca. 10 nm or short stripes, as a result the RMS roughness dramatically increases to 1.23 nm. Upon being annealed at 135 ℃ for 10 min, obviously the P3HT aggregates observed in the un-annealed P3HT:PCBRh blend film evolve to longer stripes with an average length of ca. 20 nm and an RMS roughness of 1.38 nm (images C and F in Fig. 8). Such a striped structure perturbs significantly the interpenetrating network of donor: acceptor observed in P3HT: PCBM blend film. Furthermore, the length of the stripes as the P3HT aggregates is much greater than the domain size commensurate with the exciton diffusion

length for organic semiconductors which is typically 5～10 nm, suggesting that an unfavorable exciton diffusion may occur in the P3HT:PCBRh blend films.[57-58]

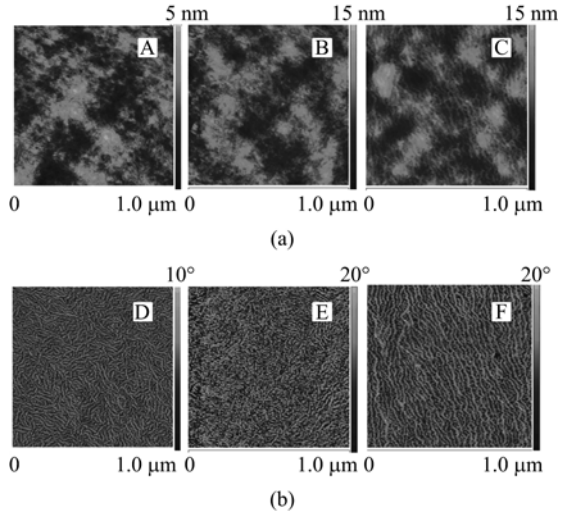

A,D: P3HT:PCBM film thermally annealed at 135 ℃ for 10 min;
B,E: P3HT:PCBR film without annealing;
C,F: P3HT:PCBR film thermally annealed at 135 ℃ for 10 min

Fig. 8　AFM height (a) and phase (b) images of blend films

It is well known that the performance of PSCs depends strongly on the nanoscale phase separation of P3HT donor and fullerene acceptor, and an interpenetrating network of donor: acceptor is desirable for maximizing their interfaces where excitons dissociate and provide pathways for transport of charge carriers to the corresponding electrode[57,59-61]. Therefore, the inferior performance of the PCBRh-based device compared to that of the reference PCBM-based one is primarily interpreted by the poor morphology of the P3HT: PCBRh blend film unfavorable for exciton diffusion and dissociation. Unexpectedly, it was reported in literatures that a thermal annealing above the glass-transition temperature (T_g) of P3HT[62-63] in a short time may improve the nanoscale phase separation of P3HT: PCBM blends[53,61], but this did not happen according to our AFM results. Besides, the poorer miscibility between PCBRh with P3HT than that between PCBM and P3HT was observed during the solution processing, and this is presumably due to the relatively lower solubility resulting from the higher tendency of aggregation of PCBRh molecules. Sufficient miscibility facilitates effective phase separation, which provides enough donor/acceptor interfaces for exciton dissociation and pathway for charge carrier transport. However, in the case of PCBRh, sulfur atom in 3-ethyl rhodanine has a strong electron-donating ability due to its large electron cloud and a small ionization energy[64], and this would result in a stronger intramolecular non-covalent interaction between C_{60} and the 3-ethyl rhodanine moiety, which may weaken the interactions of PCBRh molecules with the solvent and P3HT, and consequently result in poorer miscibility between PCBRh with P3HT. In this sense, further efficiency improvement of BHJ-PSC devices based on PCBRh acceptor could be achieved by using other donors with better miscibility and/or energy level matching PCBRh, which is now under way in our labs.

3　Conclusion

In summary, by attaching 3-ethyl rhodanine onto PCBM for the first time, we successfully synthesized a new fullerene acceptor PCBRh by a facile two-step reaction. The molecular structure of PCBRh was confirmed by ^{1}H NMR, ^{13}C NMR and MALDI-TOF mass spectroscopies. According to the UV-vis spectroscopic characterization, PCBRh shows stronger absorptions in the region of 300～600 nm than PCBM, and this is due to the high absorption coefficient of the dye unit of 3-ethyl rhodanine. Cyclic voltammetric measurement revealed that LUMO level of PCBRh is 0.1 eV higher than that of PCBM, and this can be understood by considering the electron donating property of the rhodanine moiety. Using PCBRh as an acceptor blending with P3HT, BHJ-PSC devices show a PCE of 1.46% under optimized condition (blending ratio of P3HT:PCBM = 1:1 (mass ratio), annealing treatment at 135 ℃ for 10 min), which is lower than that of reference device based on P3HT:PCBM (2.00%). AFM study of

the surface morphology of P3HT:PCBRh blend film reveals that, while in the un-annealed P3HT:PCBRh blend film P3HT aggregates into discrete spots with an average diameter ca. 10 nm or short stripes, the film upon annealing treatment at 135 ℃ for 10 min shows longer stripes with an average length of ca. 20 nm and much larger RMS roughness than that for the reference P3HT:PCBM blend film, leading to unfavorable exciton diffusion and dissociation. Furthermore, the poor miscibility between PCBRh and P3HT may prohibit efficient exciton dissociation and charge carrier transport. With the first successful incorporation of the dye unit rhodanine into fullerene acceptor, our study opens up a new avenue for the design of novel acceptor materials for PSCs.

References

[1] Lai Y Y, Cheng Y J, Hsu C S. Applications of functional fullerene materials in polymer solar cells [J]. Energy Environ Sci,2014, 7: 1 866-1 883.

[2] Krebs F C, Espinosa N, Hösel M, et al. 25th anniversary article: Rise to Power - OPV-based solar parks [J]. Adv Mater, 2014, 26(1): 29-39.

[3] Heeger A J. 25th anniversary article: Bulk heterojunction solar cells: Understanding the mechanism of operation [J]. Adv Mater, 2014, 26(1): 10-18.

[4] He Z, Wu H, Cao Y. Recent advances in polymer solar cells: Realization of high device performance by incorporating water/alcohol-soluble conjugated polymers as electrode buffer layer [J]. Adv Mater, 2014, 26(7): 1 006-1 024.

[5] Li Y. Molecular design of photovoltaic materials for polymer solar cells: Toward suitable electronic energy levels and broad absorption [J]. Acc Chem Res, 2012, 45(5): 723-733.

[6] Brabec C J, Gowrisanker S, Halls J J M, et al. Polymer - fullerene bulk-heterojunction solar cells [J]. Adv Mater, 2010, 22(34): 3 839-3 856.

[7] Cai W, Gong X, Cao Y. Polymer solar cells: Recent development and possible routes for improvement in the performance [J]. Sol Energy Mater Sol Cells, 2010, 94(2): 114-127.

[8] Krebs F C, Fyenbo J, Jorgensen M. Product integration of compact roll-to-roll processed polymer solar cell modules: Methods and manufacture using flexographic printing, slot-die coating and rotary screen printing [J]. J Mater Chem, 2010, 20(41): 8 994-9 001.

[9] Kroon R, Lenes M, Hummelen J C, et al. Small bandgap polymers for organic solar cells (Polymer material development in the last 5 years) [J]. Polymer Reviews, 2008, 48(3): 531-582.

[10] Helgesen M, Sondergaard R, Krebs F C. Advanced materials and processes for polymer solar cell devices [J]. J Mater Chem, 2010, 20(1): 36-60.

[11] He Y, Li Y. Fullerene derivative acceptors for high performance polymer solar cells [J]. Phys Chem Chem Phys, 2011, 13(6):1 970-1 983.

[12] Li C Z, Yip H L, Jen A K Y. Functional fullerenes for organic photovoltaics [J]. J Mater Chem, 2012, 22(10): 4 161-4 177.

[13] He Z, Zhong C, Su S, et al. Enhanced power-conversion efficiency in polymer solar cells using an inverted device structure [J]. Nat Photon, 2012, 6(9): 591-595.

[14] Liu S, Zhang K, Lu J, et al. High-efficiency polymer solar cells via the incorporation of an amino-functionalized conjugated metallopolymer as a cathode interlayer [J]. J Am Chem Soc, 2013, 135(41): 15 326-15 329.

[15] Hummelen J C, Knight B W, LePeq F, et al. Preparation and characterization of fulleroid and methanofullerene derivatives [J]. J Org Chem, 1995, 60(3): 532-538.

[16] Lenes M, Wetzelaer G J A H, Kooistra F B, et al. Fullerene bisadducts for enhanced open-circuit voltages and efficiencies in polymer solar cells [J]. Adv Mater, 2008, 20(11): 2 116-2 119.

[17] Meng X, Zhang W, Tan Z, et al. Dihydronaphthyl-based [60]fullerenebisadducts for efficient and stable polymer solar cells [J]. Chem Commun, 2012, 48(3): 425-427.

[18] He Y J, Chen H Y, Hou J H, et al. Indene-C(60) bisadduct: A new acceptor for high-performance polymer solar cells [J]. J Am Chem Soc, 2010, 132(4): 1 377-1 382.

[19] Kim K H, Kang H, Nam S Y, et al. Facile synthesis of o-Xylenyl fullerene multiadducts for high open circuit voltage and efficient polymer solar cells [J]. Chem Mater, 2011, 23(22): 5 090-5 095.

[20] Cheng Y J, Liao M H, Chang C Y, et al. Di(4-methylphenyl) methano-C(60) bis-adduct for efficient and sable organic photovoltaics with enhanced open-circuit voltage [J]. Chem Mater, 2011, 23(17):

4 056-4 062.

[21] Zhang C, Chen S, Xiao Z, et al. Synthesis of mono- and bisadducts of thieno-o-quinodimethane with C60 for efficient polymer solar cells [J]. Org Lett, 2012, 14(6): 1 508-1 511.

[22] Ross R B, Cardona C M, Guldi D M, et al. Endohedral fullerenes for organic photovoltaic devices [J]. Nat Mater, 2009, 8(3): 208-212.

[23] Meng X, Zhao G, Xu Q, et al. Effects of fullerene bisadduct regioisomers on photovoltaic performance [J]. Adv Funct Mater, 2014, 24(1): 158-163.

[24] Wong W W H, Subbiah J, White J M, et al. Single isomer of indene-C70 bisadduct-isolation and performance in bulk heterojunction solar cells [J]. Chem Mater, 2014, 26(4): 1 686-1 689.

[25] Wienk M M, Kroon J M, Verhees W J, et al. Efficient methano [70] fullerene/MDMO-PPV bulk heterojunction photovoltaic cells [J]. Angew Chem Int Ed, 2003, 42(29): 3 371-3 375.

[26] Wang M F, Chesnut E, Sun Y M, et al. PCBM disperse-red ester with strong visible-light absorption: Implication of molecular design and morphological control for organic solar cells [J]. J Phys Chem C, 2012, 116(1): 1 313-1 321.

[27] Mikroyannidis J A, Kabanakis A N, Sharma S S, et al. A simple and effective modification of PCBM for use as an electron acceptor in efficient bulk heterojunction solar cells [J]. Adv Funct Mater, 2011, 21(4): 746-755.

[28] Li Z, He G, Wan X, et al. Solution processable rhodanine-based small molecule organic photovoltaic cells with a power conversion efficiency of 6.1% [J]. Adv Energy Mater, 2012, 2(1): 74-77.

[29] Zhou J, Wan X, Liu Y, et al. Small molecules based on benzo[1, 2-b: 4, 5-b′]dithiophene unit for high-performance solution-processed organic solar cells [J]. J Am Chem Soc, 2012, 134(39): 16 345-16 351.

[30] Chen Y, Wan X, Long G. High performance photovoltaic applications using solution-processed small molecules [J]. Acc Chem Res, 2013, 46(11): 2 645-2 655.

[31] Fan C, Clay M D, Deyholos M K, et al. Exploration of inhibitors for diaminopimelate aminotransferase [J]. Bioorg Med Chem, 2010, 18(6): 2 141-2 151.

[32] Qu S, Li M, Xie L, et al. Noncovalent functionalization of graphene attaching [6, 6]-phenyl-C61-butyric acid methyl ester (PCBM) and application as electron extraction layer of polymer solar cells [J]. ACS Nano, 2013, 7(5): 4 070-4 081.

[33] Chen M, Li M, Wang H, et al. Side-chain substitution of poly(3-hexylthiophene) (P3HT) by PCBM via postpolymerization: An intramolecular hybrid of donor and acceptor [J]. Polymer Chemistry, 2013, 4(3): 550-557.

[34] Zhang W, Wang H, Chen B, et al. Oleamide as a self-assembled cathode buffer layer for polymer solar cells: the role of the terminal group on the function of the surfactant [J]. J Mater Chem, 2012, 22(45): 24 067-24 074.

[35] Wang H, Zhang W, Xu C, et al. Efficiency enhancement of polymer solar cells by applying poly (vinylpyrrolidone) as a cathode buffer layer via spin coating or self-assembly [J]. ACS Appl Mat Interfaces, 2012, 5(1): 26-34.

[36] Zhang W, Zhao B, He Z, et al. High-efficiency ITO-free polymer solar cells using highly conductive PEDOT: PSS/surfactant bilayer transparent anodes [J]. Energy Environ Sci, 2013, 6(6): 1 956-1 964.

[37] Zhang W, Xu Y, Wang H, et al. Fe_3O_4 nanoparticles induced magnetic field effect on efficiency enhancement of P3HT: PCBM bulk heterojunction polymer solar cells [J]. Sol Energy Mater Sol Cells, 2011, 95(10): 2 880-2 885.

[38] Wang H T, Zhang W F, Chen B X, et al. Enhancing power conversion efficiency of polymer solar cell via treatment of PEDOT: PSS anode buffer layer using DMF solvent [J]. Journal of University of Science and Technology of China, 2012, 42(10): 775-784.

[39] Zheng L, Zhou Q, Deng X, et al. Methanofullerenes used as electron acceptors in polymer photovoltaic devices [J]. J Phys Chem B, 2004, 108(32): 11 921-11 926.

[40] Wang H, He Y J, Li Y F, et al. Photophysical and electronic properties of five PCBM-like C (60) derivatives: Spectral and quantum chemical view [J]. J Phys Chem A, 2012, 116(1): 255-262.

[41] Ferraro M B, Lazzeretti P, Viglione R G, et al. Understanding proton magnetic shielding in the benzene molecule [J]. Chem Phys Lett, 2004, 390: 268-271.

[42] Zhao G, He Y, Xu Z, et al. Effect of carbon chain length in the substituent of PCBM-like molecules on their photovoltaic properties [J]. Adv Funct Mater, 2010, 20(9): 1 480-1 487.

[43] Yang S, Chen C, Liu F, et al. An improbable monometallic cluster entrapped in a popular fullerene cage: YCN@Cs(6)-C_{82} [J]. Sci Rep, 2013, 3: 1487; doi: 10.1038/srep01487.

[44] Bouit P A, Spanig F, Kuzmanich G, et al. Efficient utilization of higher-lying excited states to trigger

charge-transfer events [J]. Chem Eur J, 2010, 16(31): 9 638-9 645.

[45] Brown P, Thomas D, Köhler A, et al. Effect of interchain interactions on the absorption and emission of poly(3-hexylthiophene) [J]. Phys Rev B, 2003, 67(6): 064203;doi: 10.1103/PhysRevB.67.064203.

[46] Clark J, Silva C, Friend R H, et al. Role of intermolecular coupling in the photophysics of disordered organic semiconductors: Aggregate emission in regioregular polythiophene [J]. Phys Rev Lett, 2007, 98(20): 206406.

[47] Suzuki T, Li Q, Khemani K C, et al. Synthesis of m-phenylene- and p-phenylenebis (phenylfulleroids): Two-pearl sections of pearl necklace polymers [J]. J Am Chem Soc, 1992, 114(18): 7 300-7 301.

[48] Shi S, Khemani K C, Li Q, et al. A polyester and polyurethane of diphenyl C61: Retention of fulleroid properties in a polymer [J]. J Am Chem Soc, 1992, 114(26): 10 656-10 657.

[49] Suzuki T, Li Q, Khemani K C, et al. Systematic inflation of buckminsterfillerene C60: Synthesis of diphenyl fulleroids C61 to C66 [J]. Science, 1991, 254(5035): 1 186-1 188.

[50] Sun Q, Wang H, Yang C, et al. Synthesis and electroluminescence of novel copolymers containing crown ether spacers [J]. J Mater Chem, 2003, 13(4): 800-806.

[51] Kooistra F B, Knol J, Kastenberg F, et al. Increasing the open circuit voltage of bulk heterojunction solar cells by raising the LUMO level of the acceptor [J]. Org Lett, 2007, 9(4): 551-554.

[52] Varotto A, Treat N D, Jo J, et al. 1, 4-Fullerene derivatives: Tuning the properties of the electron transporting layer in bulk-heterojunction solar cells [J]. Angew Chem Int Ed, 2011, 50(22): 5 166-5 169.

[53] Padinger F, Rittberger R S, Sariciftci N S. Effects of postproduction treatment on plastic solar cells [J]. Adv Funct Mater, 2003, 13(1): 85-88.

[54] Troshin P A, Hoppe H, Renz J, et al. Material solubility-photovoltaic performance relationship in the design of novel fullerene derivatives for bulk heterojunction solar cells [J]. Adv Funct Mater, 2009, 19(5): 779-788.

[55] Susarova D K, Goryachev A E, Novikov D V, et al. Material solubility effects in bulk heterojunction solar cells based on the bis-cyclopropane fullerene adducts and P3HT [J]. Sol Energy Mater Sol Cells, 2014, 120: 30-36.

[56] Chen L M, Xu Z, Hong Z, et al. Interface investigation and engineering achieving high performance polymer photovoltaic devices [J]. J Mater Chem, 2010, 20(13): 2 575-2 598.

[57] Thompson B C, Frechet J M. Polymer-fullerene composite solar cells [J]. Angew Chem Int Ed, 2008, 47(1): 58-77.

[58] Scully S R, McGehee M D. Effects of optical interference and energy transfer on exciton diffusion length measurements in organic semiconductors [J]. J Appl Phys, 2006, 100(3): 034907; doi: 10.1063/1.2226687.

[59] Yang X, Loos J, Veenstra S C, et al. Nanoscale morphology of high-performance polymer solar cells [J]. NanoLett, 2005, 5(4): 579-583.

[60] Ma W, Yang C, Heeger A J. Spatial fourier-transform analysis of the morphology of bulk heterojunction materials used in "plastic" solar cells [J]. Adv Mater, 2007, 19(10): 1 387-1 390.

[61] Jo J, Kim S S, Na S I, et al. Time-dependent morphology evolution by annealing processes on polymer: Fullerene blend solar cells [J]. Adv Funct Mater, 2009, 19(6): 866-874.

[62] Zhao Y, Yuan G, Roche P, et al. A calorimetric study of the phase transitions in poly(3-hexylthiophene) [J]. Polymer, 1995, 36(11): 2 211-2 214.

[63] Ma W, Yang C, Gong X, et al. Thermally stable, efficient polymer solar cells with nanoscale control of interpenetrating network morpholoby [J]. Adv Funct Mater, 2005, 15(10): 1 617-1 622.

[64] Chen H, Peet J, Hu S, et al. The role of fullerene mixing behavior in the performance of organic photovoltaics: PCBM in low-bandgap polymers [J]. Adv Funct Mater, 2013, 24(1): 140-150.